AIAA JOURNAL
Vol. 37, No. 2, February 1999

Jet Mixing Noise from Fine-Scale Turbulence

Christopher K. W. Tam* and Laurent Auriault†
Florida State University, Tallahassee, Florida 32306-4510

It is known that turbulent mixing noise from high-speed jets consists of two components. They are the noise from large turbulent structures in the form of Mach wave radiation and the less directional fine-scale turbulence noise. The Mach wave radiation dominates in the downstream direction. The fine-scale turbulence noise dominates in the sideline and upstream directions. A semiempirical theory is developed for the prediction of the spectrum, intensity, and directivity of the fine-scale turbulence noise. The prediction method is self-contained. The turbulence information is supplied by the k–ε turbulence model. The theory contains three empirical constants beyond those of the k–ε model. These constants are determined by best fit of the calculated noise spectra to experimental measurements. Extensive comparisons between calculated and measured noise spectra over a wide range of directions of radiation, jet velocities, and temperatures have been carried out. Excellent agreements are found. It is believed that the present theory offers significant improvements over current empirical or semiempirical jet noise prediction methods in use. There is no first principle jet noise theory at the present time.

I. Introduction

SINCE the pioneering work of Lighthill,[1,2] there have been numerous attempts to develop a jet noise prediction theory. In the literature, one finds many proposed theories and semiempirical theories. The main difficulty in predicting jet noise is our lack of understanding of the turbulence in jet flows. This is true even today. However, many of the fundamental physics of jet flows that affect the propagation and radiation of jet noise were recognized very early. They have been incorporated into some of the theories. These effects include mean flow refraction[3,4] and source motion.[5] An excellent review on jet noise theories up to the late 1980s can be found in Ref. 6. References 7–9 provide reviews on the same subject. However, they include some of the more recent works, and the emphasis and perspectives are quite different.

Recently, Tam et al.[10] suggested that, because there is no intrinsic characteristic length scales and timescales in the mixing layer of a high Reynolds number jet (up to the end of the core region), not only the mean flow and the turbulence statistics must exhibit self-similarity, the same must be true for the radiated noise. By examining the entire data bank (1900 spectra in all) of the Jet Noise Laboratory of the NASA Langley Research Center, they found that turbulent mixing noise of high-speed jets consisted of two distinct components[10] (see also Ref. 9). Each component exhibits self-similarity of its own. One component radiates principally in the downstream direction. This is consistent with Mach wave radiation from the large turbulence structures/instability waves of the jet flow.[11–13] The other component that has a relatively uniform directivity is dominant in the sideline and upstream directions. These characteristics suggest that it is the noise from the fine-scale turbulence of the jet flow. Tam et al.[10] succeeded in identifying two similarity spectra from the data. They demonstrated that one of the spectra they found fitted the noise from the large turbulence structures and the other the noise from the fine-scale turbulence regardless of the jet velocity, temperature, and direction of radiation. More recently, Tam[14] showed that even the noise spectra of nonaxisymmetric jets including jets from rectangular, elliptic, plug, and suppressor nozzles fitted the same two empirically found similarity spectra. This indicates that the noise sources of these jets are similar to those of the circular jet. Their noise is also made up of two components.

The primary objective of this work is to develop a semiempirical theory for the prediction of the fine-scale turbulence noise from high-speed jets. The present theory is self-contained. The turbulence information of the jet flow needed for noise prediction are supplied by the k–ε turbulence model. Because the k–ε model is a semiempirical model, the present theory is also semiempirical. As will become clear later, the noise prediction formula developed here contains three empirical constants. These constants are determined by best fit to the noise data. Once the constants are decided, the formula can provide accurate noise spectrum and directivity predictions over the jet velocity ratio range of $u_j/a_\infty = 0.4$–3.0, where u_j and a_∞ are the fully expanded jet velocity and ambient sound speed, and temperature ratio range of $T_r/T_\infty = 1.0$–5.0, where T_r and T_∞ are the jet reservoir and ambient temperature. This parametric range brackets all known jet noise experiments and commercial jet engine operating conditions.

The use of the k–ε turbulence model to predict jet noise is not new. Khavaran et al.,[15,16] Bailly et al.,[17–19] and Bailly[20] employed the k–ε model to provide turbulence statistics to their chosen version of the acoustic analogy theory for supersonic jet noise prediction. Khavaran et al.[15,16] tuned their empirical constants to fit the measured jet noise data at Mach 1.4. However, even at this Mach number, the calculated spectra do not fit the measured data well at 90 deg and in the forward direction for which the fine-scale turbulence noise dominates. Bailly et al.[17–19] and Bailly[20] were more interested in using their model to calculate Mach wave radiation from supersonic jets. There is fair agreement between their computed and measured directivity data, but the calculated spectral distributions do not match well with experiments.

To develop a fine-scale turbulence noise theory requires many steps. We will first turn to the question of how fine-scale turbulence in a jet generates sound. For this purpose, we will use the gas kinetic theory analogy. The use of gas kinetic theory to elucidate ideas in turbulence is well established.[21] Consider the motion of gas molecules in a moving frame fixed to the mean velocity $\bar{\boldsymbol{v}}$ as shown in Fig. 1. Suppose m is the mass of a molecule, and n is the number density. Because of the random motion of the gas molecules, the gas exerts a pressure p on its surroundings. It is a simple matter to show, following standard kinetic theory of gases,[22,23] that p is given by

$$p = \tfrac{1}{3}mn\langle \boldsymbol{v}\cdot\boldsymbol{v}\rangle = \tfrac{1}{3}\rho\langle v^2\rangle \tag{1}$$

where $\boldsymbol{v}$ is the random molecular velocity, ρ is the density of the gas, and $\langle\ \rangle$ is the ensemble average.

Now we will regard fine-scale turbulence as small blobs of fluid moving randomly, as shown in Fig. 2. Again, let $\boldsymbol{v}$ be the random velocity of the fine-scale turbulence measured in the mean flow moving

Received March 25, 1998; presented as Paper 98-2354 at the AIAA/CEAS 4th Aeroacoustics Conference (AIAA 19th Aeroacoustics Conference), Toulouse, France, June 2–4, 1998; revision received Sept. 20, 1998; accepted for publication Sept. 28, 1998.

*Distinguished Research Professor, Department of Mathematics. Associate Fellow AIAA.
†Graduate Student, Department of Mathematics.

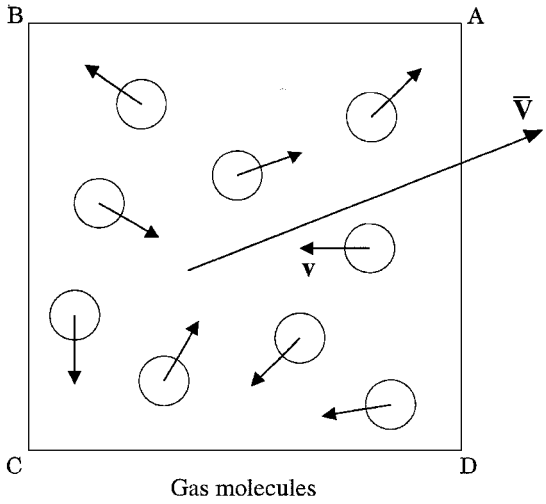

Fig. 1 Random motion of gas molecules in the moving frame fixed to the mean velocity $\bar{V}$.

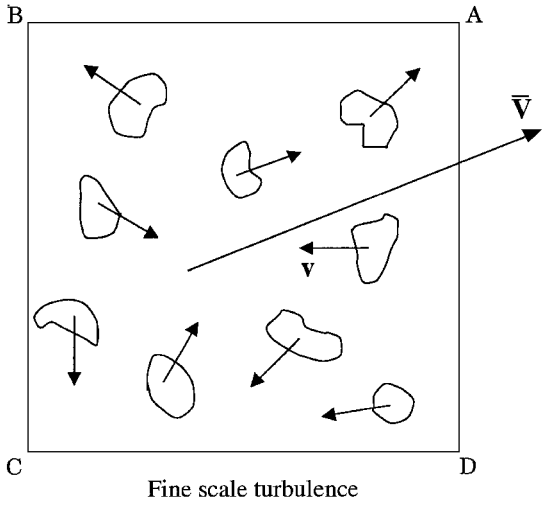

Fig. 2 Random motion of blobs of fine scale turbulent fluid in a frame of reference moving with the mean velocity $\bar{V}$.

frame. By analogy to the gas molecules of Fig. 1, the fine-scale turbulence effectively exerts a pressure p_{turb} on its surroundings. This pressure, following Eq. (1), is equal to

$$p_{\text{turb}} = q_s \equiv \tfrac{1}{3}\rho\langle v^2\rangle = \tfrac{2}{3}\rho k_s \tag{2}$$

where $k_s = \frac{1}{2}\langle v^2\rangle$ is the kinetic energy of the fine-scale turbulence per unit mass. The pressure given by Eq. (2) is a macroscopic quantity valid for length scale larger than the size of an individual blob of turbulent fluid. This pressure must be balanced by pressure and momentum flux of the surrounding fluid. If this pressure fluctuates in time, it will inevitably give rise to compressions and rarefactions in the fluid medium. This results in acoustic disturbances. Following this reasoning, one would expect the source of fine-scale turbulence noise to be equal to the time rate of change of p_{turb} or q_s in the moving frame of the fluid. In other words, Dq_s/Dt, the convective derivative of q_s, is the noise source term in a turbulent flow.

In Sec. II, the equations governing the generation and propagation of acoustic disturbances in a jet flow (generated by fine-scale turbulence) are formally derived. Here we will begin with the Reynolds averaged Navier–Stokes (RANS) equations. The relationship between the radiated sound field and the source of fine-scale turbulence noise will be established. In Sec. III, a semiempirical model of the noise source space–time correlation function is developed. The parameters of the correlation function are then related to the length scales and timescales of the k–ε turbulence model. By means of this source correlation function, a formula for the spectrum of the radiated noise is derived. Extensive comparisons between the calculated results of this formula and experimental measurements have been carried out. A sample of these comparisons are reported in Sec. IV. Good agreements are found over both subsonic and supersonic Mach number. Temperature dependence over a wide range of jet to ambient temperature ratios is also correctly predicted.

II. Formulation

Consider the flow of a turbulent compressible jet. A convenient way to account for the effect of compressibility is to use Favre average variables.[24] For the present purpose, we may regard the average as a volume average[25] with a sharp Fourier cutoff filter:

$$\bar{\phi}(x_i) = \int G\big(x_i - x_i^*, \Delta\big)\phi\big(x_i^*\big)\,\mathrm{d}^3x_i^*$$

where G is the filter function, Δ is the filter width, and

$$\int G\big(x_i - x_i^*, \Delta\big)\,\mathrm{d}^3x_i^* = 1$$

Here the filter width is chosen to be smaller than the large turbulence structures of the jet flow but larger than the fine-scale turbulence. Thus, the averaging process filters out only the small-scale turbulence.

We will decompose a flow variable into two parts,

$$f = \tilde{f} + f'' \tag{3}$$

where $\tilde{f}$ and f'' are the Favre average and Favre fluctuating components,

$$\tilde{f} = \overline{\rho f}/\bar{\rho}$$

On starting from the equations of motion and by invoking the Reynolds averaging assumption,[25] it is straightforward to derive the familiar RANS, e.g., see Ref. 26,

$$\bar{\rho}\left[\frac{\partial \tilde{u}_i}{\partial t} + \tilde{u}_j\frac{\partial \tilde{u}_i}{\partial x_j}\right] = -\frac{\partial \bar{p}}{\partial x_i} + \frac{\partial}{\partial x_j}(-\overline{\rho u_i'' u_j''} + \bar{\tau}_{ij}) \tag{4}$$

The terms $\bar{\tau}_{ij}$ and $-\overline{\rho u_i'' u_j''}$ on the right side of Eq. (4) are the viscous and Reynolds stresses, respectively. On following the generally accepted RANS approach, we will adopt the Boussinesq eddy viscosity model for the Reynolds stresses, i.e.,

$$-\overline{\rho u_i'' u_j''} = 2\mu_t\big(S_{ij} - \tfrac{1}{3}S_{kk}\delta_{ij}\big) - \tfrac{2}{3}\bar{\rho}k_s\delta_{ij} \tag{5}$$

where μ_t is the eddy viscosity and

$$S_{ij} = \frac{1}{2}\left(\frac{\partial \tilde{u}_i}{\partial x_j} + \frac{\partial \tilde{u}_j}{\partial x_i}\right) \tag{6}$$

$$\overline{\rho u_i'' u_i''} = 2\bar{\rho}k_s \tag{7}$$

Of importance is that k_s as defined by Eq. (7) is the kinetic energy of the fine-scale turbulence per unit mass.

As discussed in the preceding section, k_s in Eq. (5) effectively represents a pressure field exerted by the fine-scale turbulence on the surrounding fluid. The time fluctuation of this pressure field causes compressions and rarefactions in the fluid medium. In this way, sound is generated by the small-scale turbulence. Inside the jet flow, the acoustic field is a very small part of the unsteady fluctuations. It is sufficient to consider the acoustic field generated by the time-dependent part of k_s, denoted by $\hat{k}_s$, to be given by the linearized form of Eqs. (4) and (5). The linearization is to be performed over the mean flow of the jet. In addition, both molecular and eddy viscosity terms will be ignored as they will have only a relatively small effect on the acoustic disturbances. The linearized form of Eq. (4) with only $\hat{k}_s$ terms retained on the right-hand side, after applying the locally parallel mean flow approximation, is

$$\bar{\rho}\left[\frac{\partial u_i}{\partial t} + \bar{u}_j\frac{\partial u_i}{\partial x_j} + u_i\frac{\partial \bar{u}_j}{\partial x_j}\right] + \frac{\partial p}{\partial x_i} = -\frac{\partial q_s}{\partial x_i} \tag{8}$$

where

$$q_s = \tfrac{2}{3}\bar{\rho}\hat{k}_s \tag{9}$$

is the unsteady pressure exerted by the fine-scale turbulence. In Eq. (8), $\bar{u}_i$ and $\bar{\rho}$ are the mean velocity and density of the jet and u_i and p are the acoustic field variables associated with $\hat{k}_s$. We will now supplement Eq. (8) with the linearized continuity and energy equation (ignoring viscous and thermal dissipations) to form a closed system of equations for the acoustic field. With respect to a cylindrical coordinate system (r, ϕ, x) centered at the nozzle exit (with the x axis coinciding with the jet axis), the full set of governing equations is

$$\bar{\rho}\left[\frac{\partial u}{\partial t}+\bar{u}\frac{\partial u}{\partial x}+v\frac{\mathrm{d}\bar{u}}{\mathrm{d}r}\right]+\frac{\partial p}{\partial x}=-\frac{\partial q_s}{\partial x} \tag{10a}$$

$$\bar{\rho}\left[\frac{\partial v}{\partial t}+\bar{u}\frac{\partial v}{\partial x}\right]+\frac{\partial p}{\partial r}=-\frac{\partial q_s}{\partial r} \tag{10b}$$

$$\bar{\rho}\left[\frac{\partial w}{\partial t}+\bar{u}\frac{\partial w}{\partial x}\right]+\frac{1}{r}\frac{\partial p}{\partial \phi}=-\frac{1}{r}\frac{\partial q_s}{\partial \phi} \tag{10c}$$

$$\frac{\partial p}{\partial t}+\bar{u}\frac{\partial p}{\partial x}+\gamma\bar{p}\left[\frac{1}{r}\frac{\partial (vr)}{\partial r}+\frac{1}{r}\frac{\partial w}{\partial \phi}+\frac{\partial u}{\partial x}\right]=0 \tag{10d}$$

In these equations (u, v, w) are the velocity components in the (x, r, ϕ) directions. Also, in accordance with the locally parallel flow approximation, $\bar{\rho}$ and $\bar{u}$ are regarded as functions of r alone, and $\bar{p}=p_\infty$ is constant.

A. Acoustic Field

Equations (10a–10d), except for the noise source terms on the right, are identical to Lilley's equation.[4,6] As is well known, Lilley's approach was designed to account for the mean flow refraction effect. This effect is especially significant for the high-frequency part of the noise spectrum. This is confirmed in the numerical results reported in Sec. IV.

A formal solution of Eq. (10) directly relating the radiated acoustic pressure field to the fine-scale turbulence intensity q_s can be found by using the space–time Green's function of these equations. Because q_s appears on the right-hand side of Eqs. (10a–10c), three Green's functions are necessary. Let (u_n, v_n, w_n, p_n), with $n=1, 2,$ and 3, be the Green's functions corresponding to a source on the right-hand side of Eqs. (10a), (10b), or (10c), respectively. These Green's functions satisfy the following nonhomogeneous equations:

$$\bar{\rho}\left[\frac{\partial u_n}{\partial t}+\bar{u}\frac{\partial u_n}{\partial x}+v_n\frac{\mathrm{d}\bar{u}}{\mathrm{d}r}\right]+\frac{\partial p_n}{\partial x}=\delta(\boldsymbol{x}-\boldsymbol{x}_1)\delta(t-t_1)\delta_{n1} \tag{11}$$

$$\bar{\rho}\left[\frac{\partial v_n}{\partial t}+\bar{u}\frac{\partial v_n}{\partial x}\right]+\frac{\partial p_n}{\partial r}=\delta(\boldsymbol{x}-\boldsymbol{x}_1)\delta(t-t_1)\delta_{n2} \tag{12}$$

$$\bar{\rho}\left[\frac{\partial w_n}{\partial t}+\bar{u}\frac{\partial w_n}{\partial x}\right]+\frac{1}{r}\frac{\partial p_n}{\partial \phi}=\delta(\boldsymbol{x}-\boldsymbol{x}_1)\delta(t-t_1)\delta_{n3} \tag{13}$$

$$\frac{\partial p_n}{\partial t}+\bar{u}\frac{\partial p_n}{\partial x}+\gamma\bar{p}\left[\frac{1}{r}\frac{\partial (v_n r)}{\partial r}+\frac{1}{r}\frac{\partial w_n}{\partial \phi}+\frac{\partial u_n}{\partial x}\right]=0 \tag{14}$$

where $n=1, 2, 3$. Here $\delta(\,)$ is the Dirac delta function and δ_{nm} is the Kronecker delta. The Green's functions depend on four variables. They are the field or observer coordinates $\boldsymbol{x}$, the source coordinates $\boldsymbol{x}_1$, the field or observation time t, and the source time t_1. To avoid confusion, whenever it is necessary to display the arguments of the Green's function, they will always be in exactly this order, e.g., $p_n(\boldsymbol{x}, \boldsymbol{x}_1, t, t_1)$.

The space–time Green's function is related to the time harmonic Green's function $(\hat{u}_n, \hat{v}_n, \hat{w}_n \hat{p}_n)$ by the Fourier inverse transform. For example, we have

$$p_n(\boldsymbol{x}, \boldsymbol{x}_1, t, t_1)=\int_{-\infty}^{\infty}\hat{p}_n(\boldsymbol{x}, \boldsymbol{x}_1, \omega)\exp[-i\omega(t-t_1)]\,\mathrm{d}\omega \tag{15}$$

The equations governing the time harmonic Green's functions are simply the Fourier transforms of Eqs. (11–14). Recently the present authors[27] have shown that there is great computational advantage to using the adjoint time harmonic Green's function instead of the time harmonic Green's functions. On following the work of Ref. 27, it is easy to find that the adjoint time harmonic Green's function (u_a, v_a, w_a, p_a) (subscript a indicates the adjoint) satisfies the following equations:

$$-\bar{\rho}\left[i\omega u_a+\bar{u}\frac{\partial u_a}{\partial x}\right]-\gamma\bar{p}\frac{\partial p_a}{\partial x}=0 \tag{16}$$

$$-\bar{\rho}\left[i\omega v_a+\bar{u}\frac{\partial v_a}{\partial x}-\frac{\mathrm{d}\bar{u}}{\mathrm{d}r}u_a\right]-\gamma\bar{p}\frac{\partial p_a}{\partial r}=0 \tag{17}$$

$$-\bar{\rho}\left[i\omega w_a+\bar{u}\frac{\partial w_a}{\partial x}\right]-\frac{\gamma\bar{p}}{r}\frac{\partial p_a}{\partial \phi}=0 \tag{18}$$

$$-i\omega p_a-\bar{u}\frac{\partial p_a}{\partial x}-\left[\frac{1}{r}\frac{\partial (v_a r)}{\partial r}+\frac{1}{r}\frac{\partial w_a}{\partial \phi}+\frac{\partial u_a}{\partial x}\right]=\frac{1}{2\pi}\delta(\boldsymbol{x}-\boldsymbol{x}_1) \tag{19}$$

It is straightforward to show that the pressure fields of the three original time harmonic Green's functions are related to the adjoint Green's function by[27]

$$\begin{aligned}\hat{p}_1(\boldsymbol{x}, \boldsymbol{x}_1, \omega)&=u_a(\boldsymbol{x}_1, \boldsymbol{x}, \omega)\\ \hat{p}_2(\boldsymbol{x}, \boldsymbol{x}_1, \omega)&=v_a(\boldsymbol{x}_1, \boldsymbol{x}, \omega)\\ \hat{p}_3(\boldsymbol{x}, \boldsymbol{x}_1, \omega)&=w_a(\boldsymbol{x}_1, \boldsymbol{x}, \omega)\end{aligned} \tag{20}$$

The arguments on the two sides of Eq. (20) satisfy the reciprocity relation. That is, the source point and the field point of the adjoint are interchanged. It is clear from Eq. (20) that there is another important advantage in using the adjoint Green's function. If one is interested in the far acoustic field, namely, the pressure field, it is only necessary to solve the adjoint equations (16–19) once to obtain (u_a, v_a, w_a). On the other hand, to find $\hat{p}_1$, $\hat{p}_2$, and $\hat{p}_3$ directly, one has to solve the original time harmonic Green's function equations three times. For details of how the adjoint Green's function can be easily computed and how it accounts for the refraction effects of the jet mean flow, the readers are referred to Ref. 27.

By means of the adjoint Green's function, the pressure field generated by the source terms on the right side of Eqs. (10a–10d) is formally given by

$$\begin{aligned}p(\boldsymbol{x}, t)=-\int\int\int_{-\infty}^{\infty}\int\int\int\Bigg[&u_a(\boldsymbol{x}_1, \boldsymbol{x}, \omega)\frac{\partial q_s(\boldsymbol{x}_1, t_1)}{\partial x_1}\\ &+v_a(\boldsymbol{x}_1, \boldsymbol{x}, \omega)\frac{\partial q_s(\boldsymbol{x}_1, t_1)}{\partial r_1}+\frac{w_a(\boldsymbol{x}_1, \boldsymbol{x}, \omega)}{r}\frac{\partial q_s(\boldsymbol{x}_1, t_1)}{\partial \phi}\Bigg]\\ &\times\exp[-i\omega(t-t_1)]\,\mathrm{d}\omega\,\mathrm{d}t_1\,\mathrm{d}\boldsymbol{x}_1\end{aligned} \tag{21}$$

Let

$$\nabla_1\equiv\left(\frac{\partial}{\partial x_1}\boldsymbol{e}_x+\frac{\partial}{\partial y_1}\boldsymbol{e}_y+\frac{\partial}{\partial z_1}\boldsymbol{e}_z\right)$$

be the gradient with respect to the $\boldsymbol{x}_1$ coordinates. Equation (21) may be rewritten in the form

$$\begin{aligned}p(\boldsymbol{x}, t)=-\int\int\int_{-\infty}^{\infty}\int\int\int\{&\nabla_1\cdot[\boldsymbol{v}_a(\boldsymbol{x}_1, \boldsymbol{x}, \omega)q_s(\boldsymbol{x}_1, t_1)]\\ &-q_s(\boldsymbol{x}_1, t_1)\nabla_1\cdot\boldsymbol{v}_a(\boldsymbol{x}_1, \boldsymbol{x}, \omega)\}\exp[-i\omega(t-t_1)]\,\mathrm{d}\omega\,\mathrm{d}t_1\,\mathrm{d}\boldsymbol{x}_1\end{aligned} \tag{22}$$

where $\boldsymbol{v}_a=(u_a, v_a, w_a)$. This formula can be simplified in two ways. First, we can apply the divergence theorem to the first term of the integrand. This converts the volume integral $\mathrm{d}\boldsymbol{x}_1$ to a surface integral outside the jet flow. But q_s is zero outside the jet. Thus, there is no contribution from the first term. Now for $\boldsymbol{v}_a(\boldsymbol{x}_1, \boldsymbol{x}, \omega)$, the source is

outside the jet flow if $\boldsymbol{x}$ is in the far field. Thus, by making use of Eq. (19), Eq. (22) becomes

$$\underset{\boldsymbol{x}\text{ outside the jet}}{p(\boldsymbol{x},t)} = -\int_{-\infty}^{\infty}\iiint q_s(\boldsymbol{x}_1,t_1) \times\left[\left(i\omega+\bar{u}\frac{\partial}{\partial x_1}\right)p_a\,\exp[-i\omega(t-t_1)]\,\mathrm{d}\omega\right]\mathrm{d}t_1\,\mathrm{d}\boldsymbol{x}_1$$

$$= -\int_{-\infty}^{\infty}\iiint q_s(\boldsymbol{x}_1,t_1) \times\left[\left(\frac{\partial}{\partial t_1}+\bar{u}\frac{\partial}{\partial x_1}\right)p_a\,\exp[-i\omega(t-t_1)]\,\mathrm{d}\omega\right]\mathrm{d}t_1\,\mathrm{d}\boldsymbol{x}_1$$

Finally, by simple integration by parts, we find the desirable formula for $p(\boldsymbol{x},t)$,

$$\underset{\boldsymbol{x}\text{ outside the jet}}{p(\boldsymbol{x},t)} = \int_{-\infty}^{\infty}\iiint\left[\int_{-\infty}^{\infty} p_a(\boldsymbol{x}_1,\boldsymbol{x},\omega) \times\exp[-i\omega(t-t_1)]\,\mathrm{d}\omega\right]\frac{\mathrm{D}q_s(\boldsymbol{x}_1,t_1)}{\mathrm{D}t_1}\,\mathrm{d}t_1\,\mathrm{d}\boldsymbol{x}_1 \tag{23}$$

where

$$\frac{\mathrm{D}}{\mathrm{D}t_1}=\frac{\partial}{\partial t_1}+\bar{u}\frac{\partial}{\partial x_1}$$

is the convective derivative following the mean flow.

Equation (23) is the main result of this section. Obviously, it is open to the interpretation that noise from fine-scale turbulence is generated by the time rate of change of the turbulence kinetic energy or pressure in the moving frame following the convection of the fine-scale turbulence by the mean flow. The term inside the square bracket is the adjoint Green's function with the source located at $\boldsymbol{x}$ and the field point at $\boldsymbol{x}_1$ according to the reciprocity relation.

B. Spectral Density of the Radiated Sound

By means of Eq. (23), the autocorrelation function for a point in the acoustic far field may be formed, i.e.,

$$\langle p(\boldsymbol{x},t)p(\boldsymbol{x},t+\tau)\rangle = \int_{-\infty}^{\infty}\cdots\iint p_a(\boldsymbol{x}_1,\boldsymbol{x},\omega_1)p_a(\boldsymbol{x}_2,\boldsymbol{x},\omega_2) \times\left\langle\frac{\mathrm{D}q_s(\boldsymbol{x}_1,t_1)}{\mathrm{D}t_1}\frac{\mathrm{D}q_s(\boldsymbol{x}_2,t_2)}{\mathrm{D}t_2}\right\rangle\exp[-i\omega_1(t-t_1) - i\omega_2(t-t_2)-i\omega_2\tau]\,\mathrm{d}\omega_1\,\mathrm{d}\omega_2\,\mathrm{d}t_1\,\mathrm{d}t_2\,\mathrm{d}\boldsymbol{x}_1\,\mathrm{d}\boldsymbol{x}_2 \tag{24}$$

In Eq. (24), $\langle\,\rangle$ is the ensemble average.

The spectral density of the radiated sound $S(\boldsymbol{x},\omega)$ is the Fourier transform of the autocorrelation function or

$$S(\boldsymbol{x},\omega)=\frac{1}{2\pi}\int_{-\infty}^{\infty}\langle p(\boldsymbol{x},t)p(\boldsymbol{x},t+\tau)\rangle\,e^{i\omega\tau}\,\mathrm{d}\tau \tag{25}$$

By using

$$\int_{-\infty}^{\infty}\exp[i(\omega-\omega_2)\tau]\,\mathrm{d}\tau = 2\pi\delta(\omega-\omega_2)$$

it is straightforward to derive the following formula for $S(\boldsymbol{x},\omega)$ from Eq. (24):

$$S(\boldsymbol{x},\omega) = \int_{-\infty}^{\infty}\cdots\iint p_a(\boldsymbol{x}_1,\boldsymbol{x},\omega_1)p_a(\boldsymbol{x}_2,\boldsymbol{x},\omega_2) \times\left\langle\frac{\mathrm{D}q_s(\boldsymbol{x}_1,t_1)}{\mathrm{D}t_1}\frac{\mathrm{D}q_s(\boldsymbol{x}_2,t_2)}{\mathrm{D}t_2}\right\rangle\exp[-i(\omega_1+\omega_2)t + i\omega_1t_1 + i\omega_2t_2]\delta(\omega-\omega_2)\,\mathrm{d}\omega_1\,\mathrm{d}\omega_2\,\mathrm{d}t_1\,\mathrm{d}t_2\,\mathrm{d}\boldsymbol{x}_1\,\mathrm{d}\boldsymbol{x}_2 \tag{26}$$

III. Model Space–Time Correlation Function

To proceed further, we need a mathematical representation of the noise source space–time correlation function

$$\left\langle\frac{\mathrm{D}q_s(\boldsymbol{x}_1,t_1)}{\mathrm{D}t_1}\frac{\mathrm{D}q_s(\boldsymbol{x}_2,t_2)}{\mathrm{D}t_2}\right\rangle$$

This correlation function has never been measured before. However, the two-point space–time correlation of the fluctuating axial velocity component in jets has been measured and studied by Davies et al.[28] and Chu.[29] We believe that the mathematical form of $\langle(\mathrm{D}q_s/\mathrm{D}t_1)/(\mathrm{D}q_s/\mathrm{D}t_2)\rangle$ should be similar to that of the measured two-point space–time correlation function of the axial velocity component. Here we propose to adopt a model space-time correlation function characterized by three parameters. We will show that, with an appropriate choice of the parameters, the model function fits the measured function of Davies et al. (Fig. 3) well.

Let $\xi=x_1-x_2$, $\eta=y_1-y_2$, $\zeta=z_1-z_2$, and $\tau=t_1-t_2$. We will consider the following model function:

$$\left\langle\frac{\mathrm{D}q_s(\boldsymbol{x}_1,t_1)}{\mathrm{D}t_1}\frac{\mathrm{D}q_s(\boldsymbol{x}_2,t_2)}{\mathrm{D}t_2}\right\rangle = \frac{\hat{q}_s^2}{c^2\tau_s^2} \times\exp\left\{-\frac{|\xi|}{\bar{u}\tau_s}-\frac{\ell_n 2}{\ell_s^2}[(\xi-\bar{u}\tau)^2+\eta^2+\zeta^2]\right\} \tag{27}$$

In Eq. (27) $\bar{u}$ is the mean flow velocity or the transport velocity of the fine-scale turbulence. The three parameters of the model are ℓ_s, τ_s, and $\hat{q}_s^2$, where ℓ_s is the characteristic size of the fine-scale turbulence

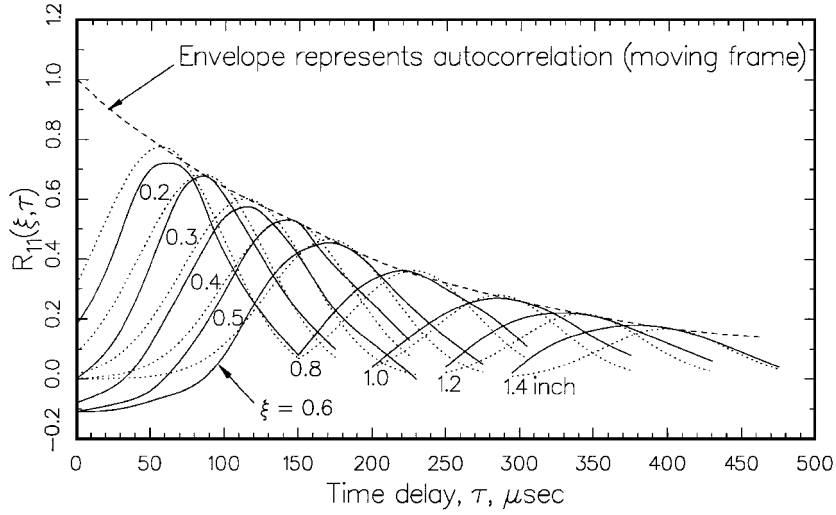

Fig. 3 Two-point space–time correlation of the axial velocity component in a jet: ——, measured data,[28] and · · · ·, model function.

in the moving frame of the mean flow, τ_s is the characteristic decay time, and $\bar{u}\tau_s$ is the decay distance. In the limit $\xi, \eta, \zeta, \tau \to 0$, Eq. (27) becomes

$$\left\langle \left(\frac{\mathrm{D}q_s(\boldsymbol{x}, t)}{\mathrm{D}t} \right)^2 \right\rangle = \frac{\hat{q}_s^2}{c^2 \tau_s^2} \tag{28}$$

Thus, $\hat{q}_s$ is a measure of the rms value of the fluctuating kinetic energy of the fine-scale turbulence and $c\tau_s$ is a typical timescale of the fluctuation. The coefficient c is expected to be less than 1.0. This indicates that the fluctuating time is shorter than the turbulence decay time.

Figure 3 shows a plot of the correlation function (27) with $\ell_s = 0.1758$ in., $\tau_s = 447.4\ \mu$s, and $\bar{u} = 3.515 \times 10^{-3}$ in./μs. As can be seen, the model function is in reasonably good agreement with the measurements of Davies et al.[28] This result assures us that the model space–time correlation function does have the right functional characteristics. We will use this model correlation function throughout this work.

Model correlation function (27) has three parameters, namely, ℓ_s, τ_s, and $\hat{q}_s$. They are the characteristic parameters of the fine-scale turbulence of the jet flow. Here we propose to obtain the values of these parameters through the k–ε turbulence model.

It is generally known that the standard k–ε turbulence model does poorly in predicting the mean flow of jets.[30] Thies and Tam[31] recognized the problem of applying the standard k–ε model to jet flows. They proposed to modify the k–ε model coefficients and showed convincingly, by comparison with a large set of jet flow data over the jet Mach number range of 0.4–2.0 and temperature ratio of 1.0 (cold jet)–4.0, that their modified k–ε model is reliable and accurate. In this work, the modified k–ε model of Ref. 31 is used.

The k–ε model provides only two pieces of information about the turbulence of the jet flow. They are the averaged turbulence kinetic energy k and the dissipation rate ε. But with k and ε known, it is possible to form a length ℓ, characterizing the size of the small-scale turbulence and a decay time τ of the turbulence as follows:

$$\ell = k^{\frac{3}{2}}/\varepsilon, \qquad \tau = k/\varepsilon \tag{29}$$

The parameters ℓ and τ of Eq. (29) are directly relevant to the parameters ℓ_s and τ_s of model two-point space–time correlation function (27). To establish their relationship, we performed a k–ε model calculation for the jet flow of the Davies et al.[28] experiment. At the location of the measured correlation function shown in Fig. 3, the value of ℓ and τ obtained were very close to 0.176 in. and 447 μs, respectively. These are the values of ℓ_s and τ_s used to match correlation function (27) to the measurements. We, therefore, believe that ℓ_s and τ_s of our model correlation function is directly related to ℓ and τ of the k–ε model. However, the k–ε model includes contributions from the large turbulence structures, whereas ℓ_s and τ_s are those of the fine-scale turbulence alone. On accounting for this difference, we propose to let

$$\ell_s = c_\ell \ell = c_\ell \left(k^{\frac{3}{2}}/\varepsilon \right), \qquad \tau_s = c_\tau \tau = c_\tau (k/\varepsilon) \tag{30}$$

where c_ℓ and c_τ ($c_\ell, c_\tau < 1.0$) are constants to be determined empirically.

Earlier we have noted that $\hat{q}_s$ is a measure of the intensity of the fluctuation of the kinetic energy of the fine-scale turbulence. We, therefore, expect it to be proportional to q, where $q = \frac{2}{3}\bar{\rho}k$. We will let

$$\hat{q}_s^2/c^2 = A^2 q^2 \tag{31}$$

where A is the third empirical constant.

With Eqs. (30) and (31), the two-point space–time correlation function (27) is known save for the three constants c_ℓ, c_τ, and A. These constants are to be determined by best fit of the calculated noise spectra to experimental measurements.

IV. Formula for the Noise Spectrum

On substitution of Eq. (27) into Eq. (26), the noise spectrum in the far field is given by

$$\begin{aligned} S(\boldsymbol{x}, \omega) = {} & \int\!\!\int_{-\infty}^{\infty} \cdots \int\!\!\int p_a(\boldsymbol{x}_1, \boldsymbol{x}, \omega_1) p_a(\boldsymbol{x}_2, \boldsymbol{x}, \omega_2) \frac{\hat{q}_s^2}{c^2 \tau_s^2} \\ & \times \exp\left\{ -\frac{|x_1 - x_2|}{\bar{u}\tau_s} - \frac{\ell n 2}{\ell_s^2} \left[(x_1 - x_2 - \bar{u}(t_1 - t_2))^2 + (y_1 - y_2)^2 \right. \right. \\ & \left. \left. + (z_1 - z_2)^2 \right] \right\} \exp[-i(\omega_1 + \omega_2)t + i\omega_1 t_1 + i\omega_2 t_2] \\ & \times \delta(\omega - \omega_2)\, \mathrm{d}t_1\, \mathrm{d}t_2\, \mathrm{d}\omega_1\, \mathrm{d}\omega_2\, \mathrm{d}\boldsymbol{x}_1\, \mathrm{d}\boldsymbol{x}_2 \end{aligned} \tag{32}$$

We will now show that most of the integrals can be evaluated analytically. The entire expression can be reduced to a single volume integral over the jet flow.

The first step is to integrate $\mathrm{d}t_1$. The integration can best be carried out by first making a change of variable to s, where

$$s = (t_1 - t_2) - \frac{(x_1 - x_2)}{\bar{u}}$$

Next, the t_2 integration can be performed resulting in $2\pi\delta(\omega_1 + \omega_2)$. With $\delta(\omega_1 + \omega_2)$ and $\delta(\omega - \omega_2)$ in the integrand, the ω_1 and ω_2 integrals can be readily evaluated giving

$$\begin{aligned} S(\boldsymbol{x}, \omega) = {} & 2\pi \left(\frac{\pi}{\ell n 2} \right)^{\frac{1}{2}} \int\!\!\int_{-\infty}^{\infty} \cdots \int\!\!\int \frac{\hat{q}_s^2}{c^2 \tau_s^2} \frac{\ell_s}{\bar{u}} \\ & \times p_a(\boldsymbol{x}_1, \boldsymbol{x}, -\omega) p_a(\boldsymbol{x}_2, \boldsymbol{x}, \omega) \exp\left[-\frac{\omega^2 \ell_s^2}{\bar{u}^2 (4 \ell n 2)} - \frac{|x_1 - x_2|}{\bar{u}\tau_s} \right] \\ & \times \exp\left\{ -\frac{\ell n 2}{\ell_s^2} \left[(y_1 - y_2)^2 + (z_1 - z_2)^2 \right] - \frac{i\omega(x_1 - x_2)}{\bar{u}} \right\} \mathrm{d}\boldsymbol{x}_1\, \mathrm{d}\boldsymbol{x}_2 \end{aligned} \tag{33}$$

In Eq. (33), the integrand is nearly zero unless $\boldsymbol{x}_1$ is close to $\boldsymbol{x}_2$. Because $\boldsymbol{x}$ is in the far field, the adjoint Green's function $p_a(\boldsymbol{x}_1, \boldsymbol{x}, -\omega)$ and $p_a(\boldsymbol{x}_2, \boldsymbol{x}, -\omega)$ differ primarily by a phase factor. The phase difference can be assessed by ray acoustics. Figure 4 shows the rays from a faraway point $\boldsymbol{x}$ to $\boldsymbol{x}_1$ and $\boldsymbol{x}_2$. The rays are essentially parallel except after entering the jet flow. We will now use a spherical polar coordinate system centered at the nozzle exit with the polar axis coinciding with the x axis, or the jet axis. Let the spherical coordinates of $\boldsymbol{x}$ be (R, Θ, ϕ), where Θ is the polar angle. The paths for the rays to $\boldsymbol{x}_1$ and $\boldsymbol{x}_2$ differ by a length nearly equal to $AC = (x_1 - x_2)\cos\Theta$ (see Fig. 4). The phase difference is equal to wave number times the difference in path lengths. Thus, the two adjoint Green's functions

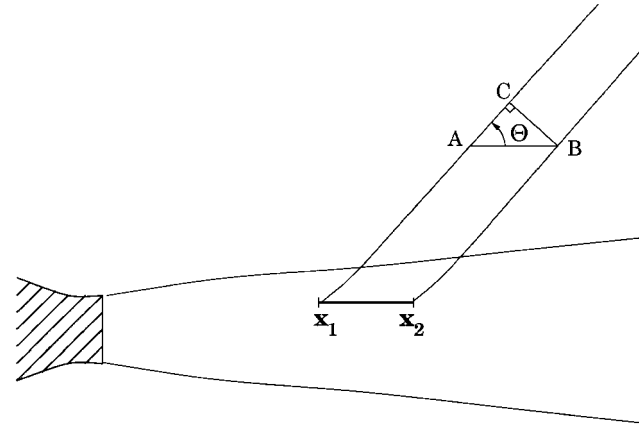

Fig. 4 Schematic diagram showing the difference in ray paths between source points x_1 and x_2 from a far-field point x with spherical coordinates (R, Θ, ϕ).

differ by a phase factor of $\exp[i(\omega/a_\infty)\cos\Theta(x_1 - x_2)]$, where a_∞ is the ambient sound speed.

We will now adopt the approximation

$$p_a(\boldsymbol{x}_1, \boldsymbol{x}, -\omega) \simeq p_a(\boldsymbol{x}_2, \boldsymbol{x}, -\omega)\exp\left[i\frac{\omega}{a_\infty}\cos\Theta(x_1 - x_2)\right] \quad (34)$$

Equation (34) may also be obtained by invoking a locally parallel flow approximation. On substitution of Eq. (34) into Eq. (33) and on noting that $p_a(\boldsymbol{x}_2, \boldsymbol{x}, -\omega) = p_a^*(\boldsymbol{x}_2, \boldsymbol{x}, \omega)$, where * indicates the complex conjugate, the integrals over $\boldsymbol{x}_1$ can be easily evaluated. This gives

$$S(\boldsymbol{x}, \omega) = 4\pi\left(\frac{\pi}{\ell n\, 2}\right)^{\frac{3}{2}} \times \int\int\int_{-\infty}^{\infty} \frac{\hat{q}_s^2 \ell_s^3}{c^2 \tau_s}\left\{|p_a(\boldsymbol{x}_2, \boldsymbol{x}, \omega)|^2 \exp\left[-\frac{\omega^2 \ell_s^2}{\bar{u}^2(4\,\ell n 2)}\right]\Big/ \times\left[1 + \omega^2\tau_s^2\left(1 - \frac{\bar{u}}{a_\infty}\cos\Theta\right)^2\right]\right\} d\boldsymbol{x}_2 \quad (35)$$

The spectral density $S(\boldsymbol{x}, \omega)$ has the dimensions of (pressure)^2 time. On converting to decibel per Strouhal number (fD_j/u_j), where u_j and D_j are the fully expanded jet velocity and diameter, the spectral density of the sound pressure field at (R, Θ, ϕ) is

$$S\left(R, \Theta, \phi; \frac{fD_j}{u_j}\right) = 10\log\left[\frac{4\pi S(\boldsymbol{x}, \omega)}{p_{\text{ref}}^2(D_j/u_j)}\right] \quad (36)$$

where p_{ref} is the reference pressure of the decibel scale.

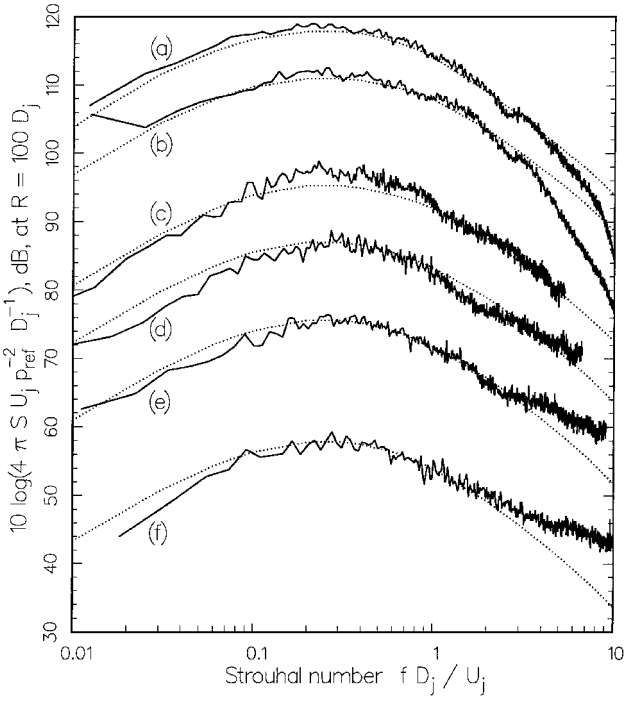

Fig. 5a Cold jet noise spectra at $\Theta = 60$ deg, $T_r/T_\infty = 1.0$, and M_j = (a) 2.0, (b) 1.49, (c) 0.9, (d) 0.7, (e) 0.5, and (f) 0.3: ——, experiments,[10,32] and · · · ·, Eq. (36).

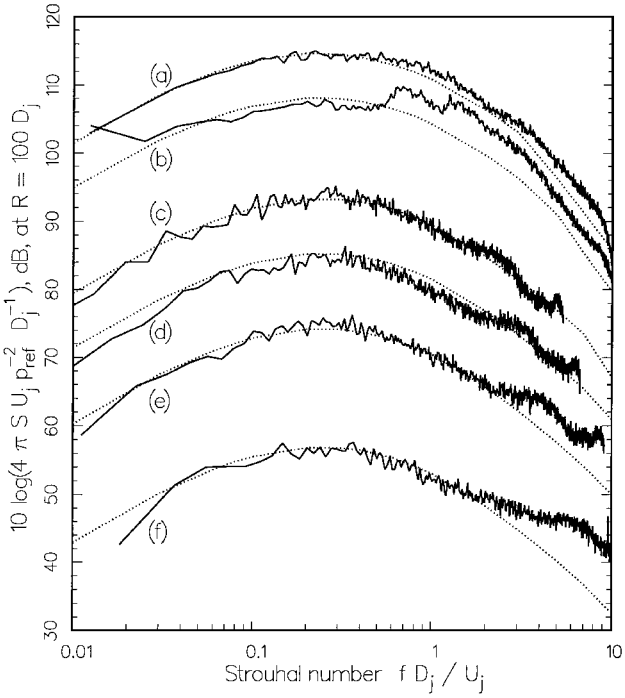

Fig. 5b Cold jet noise spectra at $\Theta = 90$ deg and $T_r/T_\infty = 1.0$.

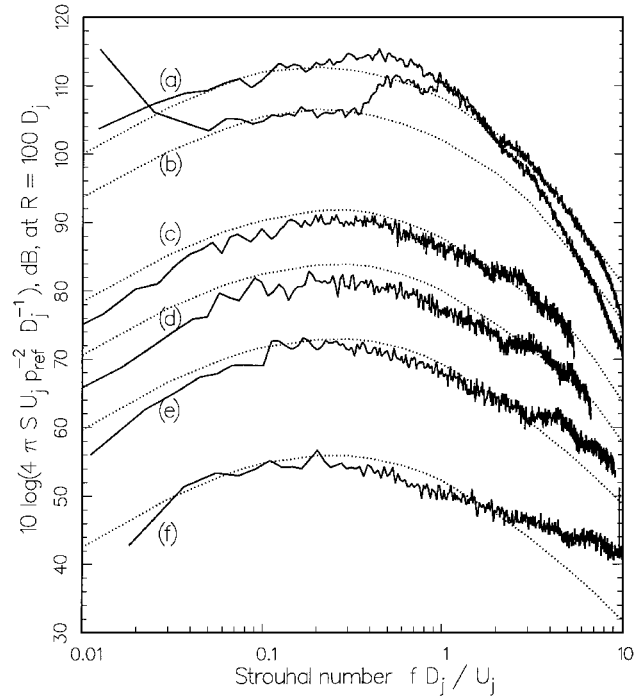

Fig. 5c Cold jet noise spectra at $\Theta = 120$ deg and $T_r/T_\infty = 1.0$.

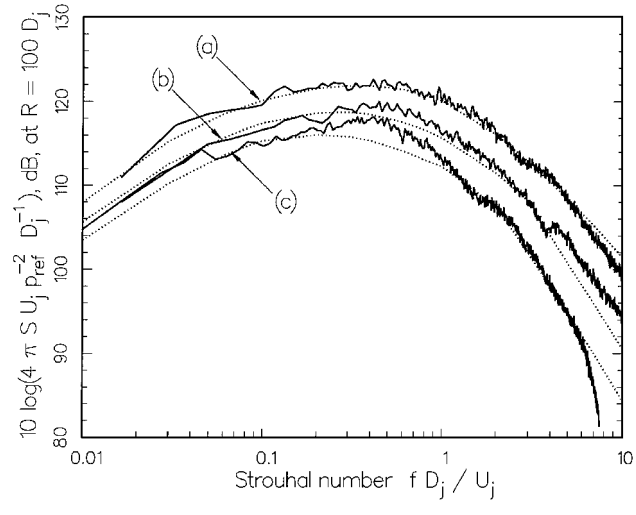

Fig. 6 Hot jet noise spectra at $M_j = 2.0$, $T_r/T_\infty = 1.8$, and Θ = (a) 69 deg, (b) 91 deg, and (c) 117 deg: ——, experiments,[10] and · · · ·, Eq. (36).

V. Comparisons with Experiments

Before we compare the numerical results of formulas (36) and (35) with experimental measurements, it is believed worthwhile to describe briefly how the various quantities and integrals of these formulas are determined and evaluated. Essentially the computations are carried out in three steps. First, with a prescribed jet operating condition, the mean flow and the values of k and ε are calculated following Ref. 31. Once k and ε are found, ℓ_s, τ_s, and $\hat{q}_s^2/c^2$ are determined by Eqs. (30) and (31). The second step is to make use of the calculated mean flow to find the adjoint Green's function as in Ref. 27. Finally, the volume integral is evaluated by dividing the jet axially into slices of 0.5 diameter. Azimuthally, the adjoint Green's function is expressed in Fourier modes. They are summed over. In the radial direction, a very fine mesh is used in the volume integration.

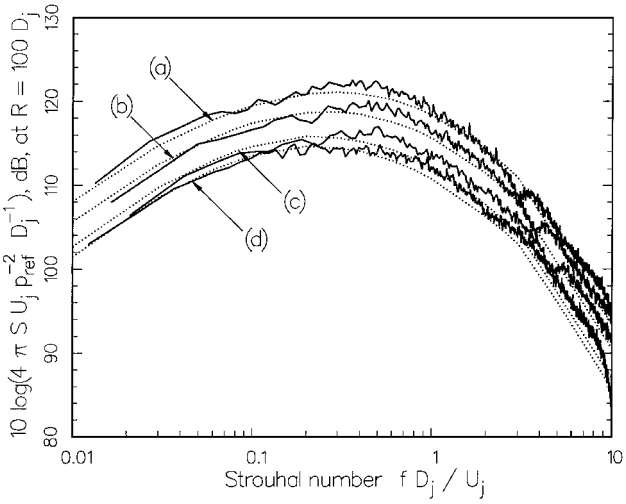

Fig. 7 Effect of jet temperature on the noise spectrum at 90 deg for a Mach 2.0 jet at T_r/T_∞ = (a) 2.72, (b) 1.8, (c) 1.12, and (d) 1.0: ——, experiments,[10] and · · · ·, Eq. (36).

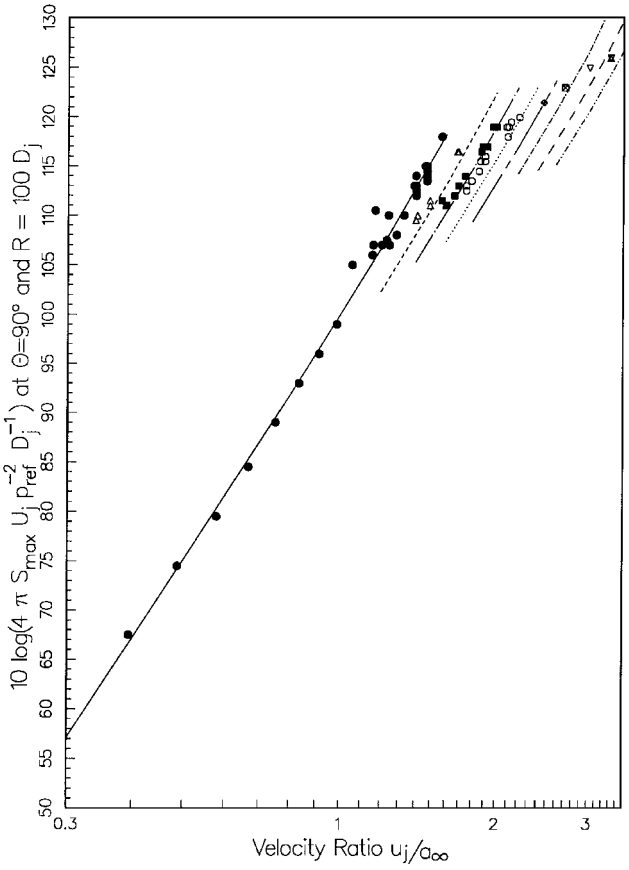

Fig. 8a Dependence of the peak level of the noise spectrum at Θ = 90 deg on velocity and temperature ratios at T_r/T_∞ = 1.0, ◗ and ——; 1.4, △ and - - - -; 1.8, ■ and —·—; 2.2, ❩ and · · · ·; 2.7, ❩ and — – —; 3.3, × and –·–·; 4.1, ▽ and — —; and 4.9, ⧖ and –··–, where symbols are measurements[10,32] and lines are Eq. (36).

We will compare formula (36) with four sets of data. They are the data of the Jet Noise Laboratory of the NASA Langley Research Center measured by Seiner and reported in Ref. 10 and the Norum and Brown,[32] Tanna et al.,[33] and Ahuja[34] data. The NASA Langley data are from supersonic jets at temperature ratio of 1.0–4.9. The Norum and Brown data include both subsonic and supersonic cold jets. The Tanna et al. data are from subsonic and supersonic jets. Only hot jet data at supersonic Mach number are considered of good quality to be included for comparison. The Ahuja data are all at subsonic Mach number at room temperature. There is overall consistency among the four sets of data. However, for hot jets at supersonic speed, the NASA data is approximately 1–2 dB higher than the Tanna et al. measurements.[33] Generally speaking, we believe that there is an uncertainty in the data of the order of 1–2 dB.

Before formulas (35) and (36) can be used, the three empirical constants c_ℓ, c_τ, and A have to be determined. After some trial and error to obtain best fit to the data, the following values are selected:

$$c_\ell = 0.256, \qquad c_\tau = 0.233, \qquad A = 0.755 \tag{37}$$

These are the values used throughout the rest of the paper.

Figures 5a–5c show comparisons of the calculated noise spectra and the experimental measurements of Refs. 10 and 32 at $T_r/T_\infty = 1.0$. The spectra are scaled to a distance of $100D_j$. Shown in Fig. 5 are data from jets at fully expanded jet Mach number $M_j = 2.0$, 1.49, 0.9, 0.7, 0.5, and 0.3. Figure 5a is for noise radiation at $\Theta = 60$ deg. As can be seen, there are excellent agreements between the calculated spectra and measurements except at very high frequency. At very high frequency, the measurements are less reliable as they are close to the high-frequency cutoff of the microphones. Figure 5b shows similar comparisons at $\Theta = 90$ deg. The agreements are again excellent except for the $M_j = 1.49$ case. The

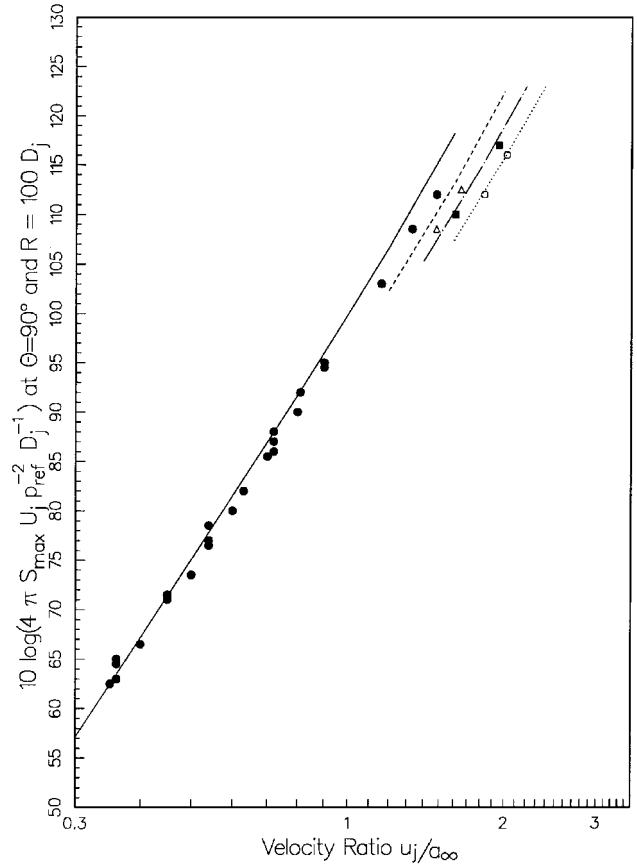

Fig. 8b Same as Fig. 8a: data from Refs. 33 and 34.

two broadband peaks on the high-frequency side of the spectrum are broadband shock associated noise.[7,8,35] They should be ignored in the comparison. In Ref. 10, this was noticed when comparing the spectrum of a perfectly expanded jet against that of an imperfectly expanded jet at identical operating conditions. Figure 5c shows the comparisons at $\Theta = 120$ deg. Again, there are good agreements. In the forward direction, most supersonic jet spectra, invariably, contain broadband shock noise. The difference between the calculated and measured spectra at $M_j = 2.0$ and 1.49 is mainly due to the presence of broadband shock associated noise.

Figure 6 shows the comparisons of hot jet spectra. The jet Mach number and temperature ratio are fixed at 2.0 and 1.8, respectively. The spectra in three directions are provided. There are good agreements between the calculated spectra and the experimental measurements. This is true both in the peak level and spectral shape. The slight difference for the case at $\Theta = 117$ deg. is again due to the presence of broadband shock associated noise in the forward direction.

To test whether formula (36) can predict accurately the change in noise spectrum with jet temperature, the noise data of Ref. 10 at Mach 2.0 in the $\Theta = 90$ deg direction are used for comparison. Figure 7 shows the calculated and measured spectra at four jet temperature ratios ranging from 1.0 to 2.72. As can readily be seen, there is again good agreement in each case.

To provide a global comparison of the calculated results of formula (36) and experimental measurements over a broad range of jet velocity and temperature, the peak value of $S(R, \Theta, \phi; fD_j/u_j)$ at $\Theta = 90$ deg are plotted in Figs. 8a and 8b as a function of u_j/a_∞. It was found in Ref. 10 that the data in such a plot tended to align themselves along nearly parallel lines according to the jet temperature ratio T_r/T_∞. Figure 8a shows the comparison between the calculated results of formula (36) and the data from Refs. 10 and 32. On considering that there is a fair amount of scattering in the experimental data, the overall agreement is excellent. Here the jet temperature ratio varies over a range of 5. This brackets all present-day commercial jet engine operating conditions. The calculated noise level and measurements are in close agreement at nearly every temperature ratio. Figure 8b shows the comparison between the calculated results and the measurements of Tanna et al.[33] and Ahuja.[34] There is a fair amount of scattering of the subsonic jet data, but they cluster around formula (36). There is also good agreement at supersonic jet velocities. As noted before, the NASA Langley Research Center data[10] are consistently 1–2 dB higher than the Tanna et al.[33] data. The calculated results appear to lie right between these two sets of measurements.

VI. Concluding Remarks

In this work a semi-empirical theory for the prediction of the fine-scale turbulence noise component of high-speed jets is developed. The fine-scale turbulence noise is the dominant noise component in the sideline and upstream directions. By comparison with experimental measurements over a wide range of jet velocity and temperature ratios, it is found that the theory can provide very accurate noise prediction.

The present theory is semiempirical. Two critical components of the theory are the model two-point space–time noise source correlation function and the k–ε turbulence model. Both models contain a fair amount of empiricism. There is, therefore, room for improvements. Theoretically, it would be desirable to be able to derive the two-point space–time correlation function from first principle and/or to replace the k–ε model by a less empirical turbulence theory. However, such an endeavor is beyond the scope of the present work.

Despite the inherent semiempirical nature of the present theory, the accuracy of the prediction over such a broad range of jet velocities and temperatures makes it superior to other methods in the literature and in practice. The present method can provide accurate spectral prediction that is vital to applications in which the use of the perceived noise level is required. The prediction of noise spectrum has proven to be most difficult in the past. Many existing theories are capable of calculating only noise intensity. From a practical standpoint, we believe the present work should be of interest to the aeroacoustics community in need of a better jet noise prediction methodology.

Acknowledgments

This work was supported primarily by NASA Grant NAG3-1683. The authors also wish to acknowledge the support of NASA Grant NAG1-1776 for C. K. W. Tam and NASA Grant NAG3-2102 for L. Auriault during the final phase of this investigation. In addition, the authors wish to thank J. M. Seiner and T. D. Norum of NASA Langley Research Center for providing additional data not appearing in their published papers.

References

[1] Lighthill, M. J., "On Sound Generated Aerodynamically: I. General Theory," *Proceedings of the Royal Society of London, Series A: Mathematical and Physical Sciences*, Vol. 211, 1952, pp. 564–581.

[2] Lighthill, M. J., "On Sound Generated Aerodynamically: II. Turbulence as a Source of Sound," *Proceedings of the Royal Society of London, Series A: Mathematical and Physical Sciences*, Vol. 222, 1954, pp. 1–32.

[3] Atvars, J., Schubert, L. K., and Ribner, H. S., "Refraction of Sound from a Point Source Placed in an Air Jet," *Journal of the Acoustical Society of America*, Vol. 37, 1965, pp. 168–170.

[4] Lilley, G. M., "On the Noise from Jets," *Noise Mechanisms*, CP-131, AGARD, 1974, pp. 13.1–13.12.

[5] Ffowcs-Williams, J. E., "The Noise from Turbulence Convected at High-Speed," *Philosophical Transactions of the Royal Society of London, Series A: Mathematical and Physical Sciences*, Vol. 255, 1963, pp. 469–503.

[6] Lilley, G. M., "Jet Noise Classical Theory and Experiments," *Aeroacoustics of Flight Vehicles: Theory and Practice*, edited by H. H. Hubbard, Vol. 1, NASA RP-1258, 1991, pp. 211–289.

[7] Tam, C. K. W., "Jet Noise Generated by Large Scale Coherent Motion," *Aeroacoustics of Flight Vehicles: Theory and Practice*, edited by H. H. Hubbard, Vol. 1, NASA RP-1258, 1991, pp. 311–390.

[8] Tam, C. K. W., "Supersonic Jet Noise," *Annual Review of Fluid Mechanics*, Vol. 27, 1995, pp. 17–43.

[9] Tam, C. K. W., "Jet Noise: Since 1952," *Theoretical and Computational Fluid Dynamics*, Vol. 10, 1998, pp. 393–405.

[10] Tam, C. K. W., Golebiowski, M., and Seiner, J. M., "On the Two Components of Turbulent Mixing Noise from Supersonic Jets," AIAA Paper 96-1716, May 1996.

[11] Tam, C. K. W., and Morris, P. J., "The Radiation of Sound by the Instability Waves of a Compressible Plane Turbulent Shear Layer," *Journal of Fluid Mechanics*, Vol. 98, 1980, pp. 349–381.

[12] Tam, C. K. W., and Burton, D. E., "Sound Generated by Instability Waves of Supersonic Flows. Part 1, Two-Dimensional Mixing Layer; Part 2, Axisymmetric Jets," *Journal of Fluid Mechanics*, Vol. 138, 1984, pp. 249–295.

[13] Tam, C. K. W., and Chen, P., "Turbulent Mixing Noise from Supersonic Jets," *AIAA Journal*, Vol. 32, No. 9, 1994, pp. 1774–1780.

[14] Tam, C. K. W., "Influence of Nozzle Geometry on the Noise of High-Speed Jets," *AIAA Journal*, Vol. 36, No. 8, 1998, pp. 1396–1400.

[15] Khavaran, A., Krejsa, E. A., and Kim, C. M., "Computation of Supersonic Jet Mixing Noise from an Axisymmetric CD Nozzle Using k–ε Turbulence Model," AIAA Paper 92-0500, Jan. 1992.

[16] Khavaran, A., Krejsa, E. A., and Kim, C. M., "Computation of Supersonic Jet Mixing Noise for an Axisymmetric Convergent-Divergent Nozzle," *Journal of Aircraft*, Vol. 31, No. 5, 1994, pp. 603–609.

[17] Bailly, C., Bechara, W., Lafon, P., and Candel, S., "Jet Noise Predictions Using a k–ε Turbulence Model," AIAA Paper 93-4412, Oct. 1993.

[18] Bailly, C., Lafon, P., and Candel, S., "Computation of Subsonic and Supersonic Jet Mixing Noise Using a Modified k–ε Model for Compressible Free Shear Flows," *Acta Acustica*, Vol. 2, April 1994, pp. 101–112.

[19] Bailly, C., Candel, S., and Lafon, P., "Prediction of Supersonic Jet Noise from a Statistical Acoustic Model and a Compressible Turbulence Closure," *Journal of Sound and Vibration*, Vol. 194, 1996, pp. 219–242.

[20] Bailly, C., "A Statistical Description of Supersonic Jet Mixing Noise," AIAA Paper 97-1575, May 1997.

[21] Tennekes, H., and Lumley, J. L., *A First Course in Turbulence*, MIT Press, Cambridge, MA, 1978, Chap. 2.

[22] Feynman, R. P., Leighton, R. B., and Sands, M., *The Feynman Lectures on Physics*, Vol. 1, Addison–Wesley, New York, 1963, Chap. 39.

[23] Liepman, H. W., and Roshko, A., *Elements of Gasdynamics*, Wiley, New York, 1957, Chap. 14.

[24] Favre, A., "Equations des Gaz Turbulents Compressibles," *Journal de Mecanique*, Vol. 3, 1965, pp. 361–390.

[25] Speziale, C. G., "Turbulence Modeling for Time Dependent RANS and VLES: A Review," *AIAA Journal*, Vol. 36, No. 2, 1998, pp. 173–184.

[26] Knight, D. D., "Numerical Simulation of Compressible Turbulent Flows Using the Reynolds-Averaged Navier–Stokes Equations," AGARD Rept. R-819, 1997.

[27] Tam, C. K. W., and Auriault, L., "Mean Flow Refraction Effects on Sound Radiated from Localized Sources in a Jet," *Journal of Fluid Mechanics*, Vol. 370, Sept. 1998, pp. 149–174.

[28]Davies, P. O. A. L., Fisher, M. J., and Barratt, M. J., "The Characteristics of the Turbulence in the Mixing Region of a Round Jet," *Journal of Fluid Mechanics*, Vol. 15, 1963, pp. 337–367.

[29]Chu, W. T., "Turbulence Measurements Relevant to Jet Noise," Inst. for Aerospace Studies, UTIAS Rept. No. 119, Univ. of Toronto, Toronto, ON, Canada, Nov. 1966.

[30]Pope, S. B., "An Explanation of the Turbulent Round Jet/Plane-Jet Anomaly," *AIAA Journal*, Vol. 16, No. 3, 1978, pp. 279–281.

[31]Thies, A. T., and Tam, C. K. W., "Computation of Turbulent Axisymmetric and Nonaxisymmetric Jet Flows Using the $k-\varepsilon$ Model," *AIAA Journal*, Vol. 34, No. 2, 1996, pp. 309–316.

[32]Norum, T. D., and Brown, M. C., "Simulated High Speed Flight Effects on Supersonic Jet Noise," AIAA Paper 93-4388, Oct. 1993.

[33]Tanna, H. K., Dean, P. D., and Burrin, R. H., "The Generation and Radiation of Supersonic Jet Noise, Vol. 3, Turbulent Mixing Noise Data," Air Force Aero Propulsion Lab., AFAPL-TR-76-65, Wright–Patterson AFB, OH, June 1976.

[34]Ahuja, K. K., "Correlation and Prediction of Jet Noise," *Journal of Sound and Vibration*, Vol. 29, 1973, pp. 155–168.

[35]Tam, C. K. W., "Broadband Shock Associated Noise of Moderately Imperfectly Expanded Supersonic Jets," *Journal of Sound and Vibration*, Vol. 140, 1988, pp. 55–71.

M. Samimy
Associate Editor